Acceleration Effects on Instability of High-Pressure Fuel Jets

D. Jarrahbashi[1] and W. A. Sirignano
Department of Mechanical and Aerospace Engineering
University of California-Irvine
Irvine, CA 92797 USA

Abstract

The transient behavior of the jet during the start-up and shut-down portion of the injection at very high Reynolds and Weber numbers is addressed in the present work. The acceleration of the liquid during start-up is about 10^6 m/s^2 at the orifice exit for high Reynolds numbers. The influence of acceleration on the dynamics of jets has never been fully considered previously. When the jet emerges from the orifice, drag forces due to the dense ambient air cause a deceleration. Also, the dynamic protrusions from the jet surface created by Kelvin-Helmholtz (KH) instability are subject to local accelerations. The Rayleigh-Taylor (RT) instabilities are driven by acceleration when the liquid accelerates away from the gas locally. With this instability, the waves corrugate at the free surface during acceleration. Ultimately, these waves will finger into the liquid, causing it to break up. The effects of the RT and KH instabilities on jet break-up during start-up and shut-down transient are considered in this research. During start-up and shut-down, the jet exit velocity varies producing an acceleration which enters into the equations of motion transferring from the laboratory frame to an accelerating frame fixed to the liquid mass center as a generalized body force. In addition, the fingers have an accelerating motion, even during steady injection. At very high Reynolds and Weber numbers, calculations show that the unstable wavelengths could be as small as a few microns. To tackle the resolution problem and capture the shortest unstable surface wavelengths, we examine stream-wise segments of the jet, treating these segments as ballistic slugs coming from the orifice. This slug or liquid section of the jet deforms and exchanges both mass and momentum with the surrounding gas during start-up and shut-down. Use has been made of the unsteady multidimensional code with a finite-volume solver of the Navier-Stokes equations for liquid streams and adjacent gas, a boundary-fitted-gridding scheme, and a level-set method for gas/liquid interface tracking. We also simulate the full transient jet during the transients. These results have been very fruitful for an estimate of the acceleration and also for implementing the proper boundary conditions in the liquid-section model. The effects of the acceleration on the surface instability and the range of unstable wavelengths in the liquid-section model have been compared with the classical instability theories.

Introduction

Understanding, insights, and quantitative descriptions are needed to explain the factors that relate to the mechanisms for the break-up of injected liquid streams at high pressure during transients (e.g., start-up and shut-down). The duration of the start-up and shut-down periods of jet injection will vary from ten to fifty percent of the injection duration, being higher at lighter loads. In other words, considering fifty percent of the injection duration, if the velocity variation were linear in time, the volume of liquid injected in the transient portions would be one-half of the volume injected during the steady portion. At heavy load (i.e., high power) and about 2000 rpm, with jet velocity about 300-400 m/s the transient period of injection is 0.25 to 0.33 ms. So, clearly transient behavior must be emphasized. Determinations of wavelengths of instabilities and resulting dimensions of ligaments and droplets breaking from the stream are desired to estimate or predict droplet-size distribution. Mechanisms for wave instabilities on the liquid-gas interface that must be analyzed and understood are capillary instability, Rayleigh-Taylor (RT) instability caused by acceleration of the interface, and Kelvin-Helmholtz (KH) instability caused by relative motion of the two phases parallel to the interface. Nonlinear growth and distortion of these surface waves lead to protrusions of liquid into the surrounding; these protrusions are commonly named "fingers". It is also necessary to understand the mechanisms which cause the fingers to break into ligaments and/or droplets that separate from the original jet (i.e., spray formation). Experience is that the liquid forms nonlinear instability waves of moderate wavelength on the liquid surface due to the KH and capillary mechanisms. As these waves grow and distort into protrusions (fingers), they accelerate relative to the surrounding gas. Consequently, smaller wavelength instabilities may form on these fingers due to RT instability. It is essential to have a good prediction of unstable surface wavelengths because these lengths can be important in determining final droplet and ligament sizes. Extremely good computational resolution is demanded in order

[1*]Corresponding author

to resolve the relevant wavelengths and to have a final break-off which is not mesh-size dependent. Numerous experimental techniques with various precisions have been used to capture the jet dynamics during the transient portion of injection. However, the complicated structures of the liquid jet surface, very close to the nozzle, together with the dense cloud of droplets in that region makes the optical access to the jet very difficult. On the other hand, very small length and time scales of atomization process cause another challenge in visualizing the liquid/gas interface. There is a lack of knowledge regarding the mixture; especially, very close to the nozzle exit during the first few seconds of the jet injection. Most of the numerical methods using the subgrid models lack the required resolution for capturing very small-scale wavelengths during start-up and shut-down. This shortcoming has been indicated by Hermann [1] and Goroshovski *et al.* [2]. They used the Refined Level Set Grid (RLSG) method to simulate the primary break-up process of liquid jets and sheets since liquid break-up predictions will be mesh size dependent.

Linne *et al.* [3] investigated the behavior of a single diesel spray during the injection process via ballistic imaging techniques. Their results confirmed the appearance of periodic structures, distinct and intermittent voids at the interface very close to the nozzle. Sazhin *et al.* [4] predicted the transient jet break-up length and its penetration into the gas by modifying the break-up model previously used for steady jet. Their results showed better agreement with the experimental data compared with the other break-up models. From their investigations, the value of acceleration indicates the time required for the amplitudes and wavelengths of the unstable waves to reach the critical criterion for break-up.

Studying the mechanism involved in secondary instability and break-up of droplets due to acceleration could be very promising to predict the effects of acceleration on liquid streams. In most of the works the droplet is accelerated either by a shock wave or a constant body force similar to gravity. Joseph *et al.* [5] investigated the secondary break-up of both Newtonian and non-Newtonian droplets in a shock tube exposed to very high accelerations. They claimed that the RT instability is the main cause of the break-up. Han *et al*. [6] performed a numerical simulation of the secondary break-up of droplets exposed to constant body force acceleration for low-density ratios. They added a body force to the axisymmetric Navier-Stokes equations to simulate the effects of constant acceleration on droplet surface. They claimed that acceleration controls the break-up mechanism when the viscous effects are negligible and surface tension is constant. The study of the break-up mode revealed that the drop is deformed in to a very thin film pulled in the downstream direction for higher accelerations; that is an indication of the shear break-up mode. Varga *et al.* [7] described the break-up of a small diameter liquid jet exposed to high-speed gas as secondary RT instability of primary KH instability. They proposed a phenomenological break-up model for the initial droplet size based on the same acceleration mechanism that breaks up liquid drops in high-speed air stream.

Investigating the effects of acceleration, i.e., RT instability on jet break-up is the main goal of the present work. Use will be made of time-dependent, axysimmetric CFD code combined with level-set method to solve the Navier-Stokes (NS) equations with continuous velocity variations across the interface and a pressure jump related to surface tension and local surface curvature. The valuable information obtained from the full transient jet [8] has been used to develop a new model to capture the instabilities at the liquid/gas interface with better resolution which would be extremely costly if a full jet was considered numerically. In this new model, a section of the jet whose fixed length is longer than interesting wavelengths but still computationally manageable will be considered. Some comparisons with the classical instability theories will be made to verify the usefulness of the Liquid-Segment model for the various configurations and conditions under study.

Numerical Methods

The Navier-Stokes equations for an incompressible flow follows:

$$\rho\frac{\partial\vec{u}}{\partial t}+\rho\vec{u}\cdot\nabla\vec{u}=-\nabla p+\mu\nabla^2\vec{u}+\vec{F};\qquad \nabla\cdot\vec{u}=0 \tag{1}$$

where $\vec{u}$ is the velocity field; ρ and μ are the density and viscosity of the fluid, respectively. p is the pressure, and F is the body force applied to the fluid. We consider a finite volume discretization on a staggered grid. The convection-diffusion problem has been discretized based on the finite volume method using the QUICK algorithm [9] and the Crank-Nicolson scheme for discretizing the unsteady term. The coupling of the continuity and momentum equations is done through the SIMPLE algorithm [10].The level-set method developed by Sussman *et al.* [11] and Osher and Fedkiw [12] is used for tracking the liquid/gas interface. Level-set is defined as a distance function with zero value at the liquid/gas interface; positive values in the gas and negative values in the liquid phase. The level-set function is denoted by θ and all the fluid properties for both phases in the Navier-Stokes equations can be defined based on their values and the equations could be solved for both phases simultaneously. The level-set function is also convected by the unknown velocity field based on the following equation:

$$\frac{\partial \theta}{\partial t} + \vec{u} \cdot \nabla \theta = 0 \tag{2}$$

In addition, the surface tension force applied on the interface is defined based on the level-set function and curvature of the interface as is shown in the third term on the right-hand side of Navier-Stokes equation as follows:

$$\rho \frac{D\vec{u}}{Dt} = -\nabla p + \mu \nabla^2 \vec{u} - \sigma \kappa \delta(d) \vec{n}. \tag{3}$$

where σ is the surface tension coefficient, δ is the delta function, n and κ are the normal vector directing toward the gas phase, and the curvature of the interface, respectively and d represents the distance from the interface. For detailed description on level-set method and delta function see Dabiri *et al.* [13, 14.]

The computational domain and gridding system that consists of an orifice initially full of liquid and a gas chamber initially filled with quiescent gas is demonstrated in Figure 1(a). The plenum pressure upstream in the orifice is prescribed to increase exponentially over a period of 0.3 ms until a prescribed maximum pressure is reached after which the plenum pressure is held constant at that cap value for another 0.1 ms. The plenum pressure drives the flow and the mass flux and the exit velocity of the jet increase with the plenum pressure. At the end of start-up process, the maximum jet velocity reaches 200 m/s. No-slip boundary condition on the orifice channel wall and slip condition on the top wall of the gas chamber have been applied. The velocity and viscous stresses are continuous at the liquid/gas interface. The computational gird consists of 2700 and 900 points in the x and r-direction, respectively from which 9600 points lie in the orifice and orifice channel. The flow properties are summarized in Table 1. Re and We numbers have been defined as follows: $Re = \frac{\rho_l \bar{u} D}{\mu_l}$, $We = \frac{\rho_l \bar{u}^2 D}{\sigma}$, where $\bar{u}$, ρ_l, μ_l, σ, and D are the maximum jet exit velocity, the liquid density, liquid viscosity, the surface tension coefficient, and the orifice diameter, respectively. The numerical simulation of the full jet at different flow conditions will be illustrated in the next section.

These results can be used to develop a new model to capture the instabilities at the liquid/gas interface with better resolution. This would be extremely costly if a full jet was considered numerically, especially, for predicting the jet instability during steady-state followed by the shut-down process. For this purpose, the length of the gas chamber must be more than 200 times the orifice diameter which would increase the cost of the simulations significantly; consequently, the required resolution for capturing very small-scale wavelengths at the interface cannot be provided considering the long computational domain.

The valuable information obtained from the full transient jet simulations described above has been used to develop a new model to capture the instabilities at the liquid/gas interface with better resolution and lower cost than for full jet computations. In this new model, a section of the jet whose fixed length is longer than interesting wavelengths but still computationally manageable, e.g., 1-mm length for a 200-micron initial diameter will be considered during the start-up and shut-down periods of jet injection. During start-up, we can expect an increasing orifice exit velocity with time, which implies a stream-wise decreasing velocity through the jet. During shut-down, there will be a temporal deceleration with a streamwise acceleration. When the jet emerges from the orifice, drag forces due to entry into the dense air cause a deceleration. Also, the dynamic protrusions from the jet surface are subject to a high acceleration. To consider the effects of this acceleration on the fluid motion, we transfer the frame of reference from the laboratory frame to an accelerating frame fixed to the liquid. This transformation generates a new term $\rho \vec{V}$ as a generalized body force analogous to gravity in the equations of motion as is shown in (4). Here, $\vec{V}$ is the constant acceleration of the frame of reference equivalent to the acceleration of the liquid jet emerging from the orifice, averaged over 300 μs after the start of injection, i.e., start-up. In the case of RT instability, $\rho \vec{V}$ is the local normal component at the liquid interface of the relevant quantity.

$$\rho \frac{D\vec{U}}{Dt} = -\nabla p + \mu \nabla^2 \vec{U} - \sigma \kappa \delta(d) \vec{n} - \rho \vec{V} \qquad \nabla \cdot \vec{U} = 0 \tag{4}$$

The fluid section consists initially of two concenteric cylinders; liquid is in the inner cylinder and the gas fills the surrounding outer cylinder. The diameters of the inner and outer cylinders are 200 and 800 μm, respectively, and the length of the liquid segment is 1 mm. The liquid section diameter is consistent with the jet-

orifice diameter used in full jet simulation. The total number of mesh points is 400,000 (1000 in x-direction and 400 in r-direction); a uniform mesh ($\Delta x=\Delta r=1\mu m$) has been used (see Figure 1(b).) Use will be made of the same axisymmetric, unsteady, finite-volume Navier-Stokes CFD solver, with the QUICK scheme and level-set method for tracking the interface used for full jet simulations considering the effects of constant body force mentioned in (4). The liquid is initially stationary and the gas flows over the interface from right to left with a starting value associated with the velocity of the liquid jet on the axis of symmetry obtained from a full jet analysis when the jet has penetrated about 1 mm into the gas. The periodic conditions for pressure and velocity at the right and left boundaries and symmetry boundary condition at the bottom of the computational domain have been applied. In addition, the normal gradient of velocity is zero on the top boundary. The flow conditions are the same as the full transient jet (see Table 1.)

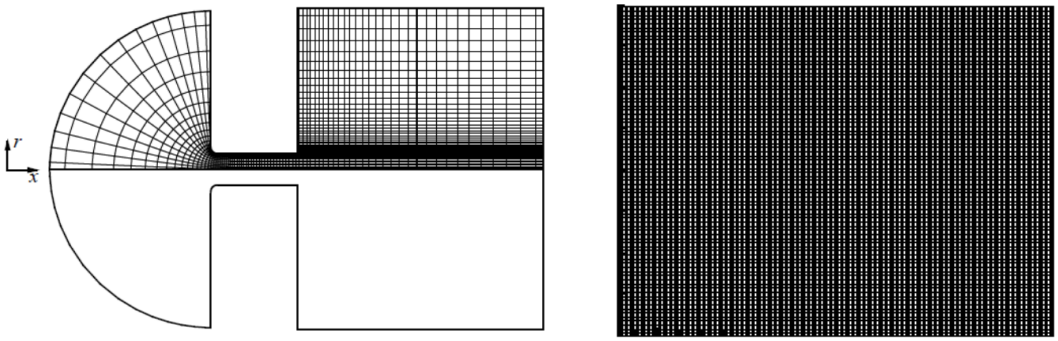

(a) (b)

Figure 1. Physical domain and orthogonal grid (a) full jet (flow from left to right), (b) liquid-segment model.

Table 1. Fluid Properties.

Fluid properties	Liquid (Kerosene)	gas (air)
Viscosity (kg/m.s)	2.7 e-3	1.8 e-5
Density (kg/m^3)	804	38.4 at 30 atm
Surface tension coefficient (N/m)	0.028	-
Maximum jet velocity (m/s)	200	-

Results and Discussion

Figure 2 illustrates the effects of liquid viscosity and surface tension on the jet development for the same pressure difference at the orifice exit at the same instant of time. The viscosity of the liquid in Figure 2(a) is 10 times that of 2(b) and 2(c). The Re number based on the maximum jet velocity is 1600 for (a) and 16000 in (b) and (c). The discrepancies between the jet penetration and unstable structures at the liquid/gas interface in Figure 2(a) and 2(b) are significant. For higher liquid viscosity, the starting liquid jet forms a cap which grows in volume as it moves downstream and decelerates along the gas chamber. At the same time, air is entrained and circulated at the back of the cap.

Due to the drag forces acting on the bulk accumulated liquid in the jet cap, the jet centerline velocity decreases drastically in the x-direction as Figure 3 depicts. However, for lower liquid viscosity shown in Figure 2(b), the mushroom-shaped cap disappears after a few microseconds after the start of injection and well-known KH and RT inabilities appear on the liquid/gas interface. This is consistent with what has been observed experimentally for a liquid jet that breaks up before a cap is formed at high Re and We numbers [14]. Based on the results shown in Figure 3, the jet tip moves approximately at the speed equal to the jet exit velocity and the effects of drag forces are negligible in the downstream direction for higher Re numbers. In other words, the acceleration of the jet exit velocity is immediately translated to all parcels in the liquid core. This essentially portrays any element of mass as a ballistic slug of liquid following a constant velocity with time; i.e., the Lagrangian time derivative is zero although velocity spatially varies in the downstream direction. Thus, we can examine stream-wise segments of the jet, treating these segments as ballistic slugs coming from the orifice instead of simulating the full jet. We will discuss this model at the end of this section.

The effects of surface tension on jet instability have been shown in Figure 2(b) and 2(c). The surface tension coefficient in 2(b) is 10 times that of 2(c). As was expected from potential flow analysis, the surface tension has stabilizing effects for high jet velocity and high Re numbers [15]. Clearly, by decreasing the surface tension, smaller wavelengths have appeared at the liquid/gas interface while the jet length remains constant. Thus, for the range of Re and We numbers that we are considering, we expect small-scale wavelengths and protrusions that become even smaller due to exposure to high accelerations normal to their interface.

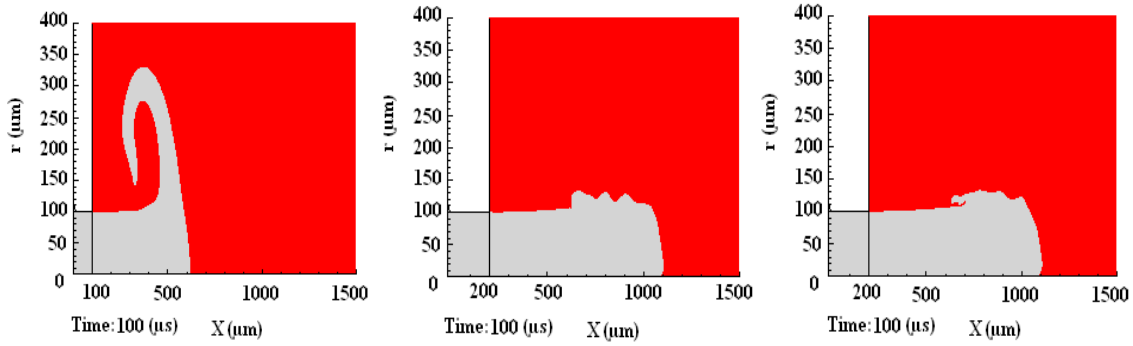

Figure 2. Effects of liquid viscosity and surface tension at 100 μs after the start of injection. (a) Re=1600, We=23,000, (b) Re=16,000, We=23,000, (c) Re=16,000, We=230,000.

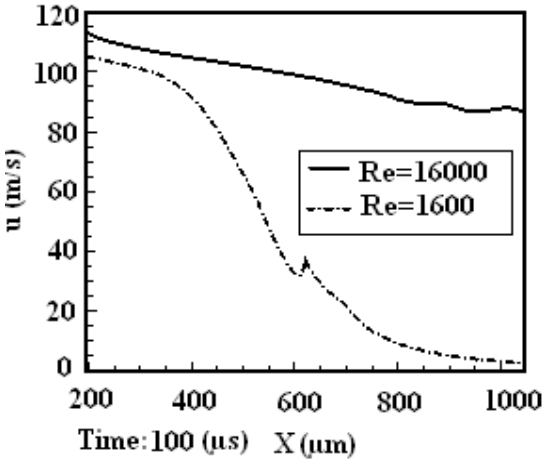

Figure 3. The difference between ambient gas and centerline velocity with downstream distance for different Re numbers.

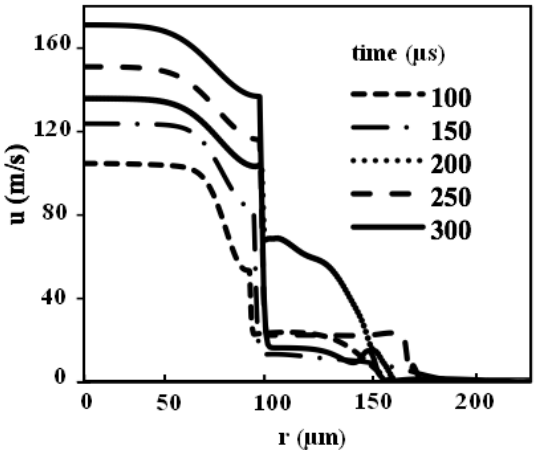

Figure 4. Velocity profile of liquid jet and surrounding gas at different instants of injection during start-up.

The jet velocity profile at the orifice exit with respect to radial direction at different instants of injection during start-up has been shown in Figure 4. The velocity of the core region of the jet is maximum on the axis of symmetry and remains constant for a distance up to half of the orifice radius and decreases sharply to match the quiescent air above that. In addition, the maximum jet velocity accelerates during the start-up. The jet acceleration depends on different parameters: namely, the Re number, orifice radius, gas density, and the pressure difference along the orifice that indicates the amount of mass emerging from the orifice during start-up. The average liquid jet acceleration is about 400,000 m/s^2 during the start-up period. The protrusions illustrated in Figure 2 are also exposed to even higher acceleration normal to their surface when drawn out of the liquid. The information obtained above has been used in developing a new model to consider the effects of acceleration providing better resolution that cannot be obtained for full jet simulations, especially, for higher Re and We numbers associated with short wavelength instabilities. The axial velocity of selected elements of mass at the nozzle exit vs. time is shown in Figure 5. This graph demonstrates the axial-velocity at different positions along the gas chamber with respect to time of injection. During the shut-down period (400<t<500 μs), the centerline velocity decreases from maximum velocity but does not reach zero in this flow configuration. As Figure 6 graphs, the instabilities that were initiated prior to the beginning of the shut-down period have endured. The jet is continuing to be extended during the shut-down although the local flow rate is now decreasing with downstream distance implying that mass is accumulating in the forward part of the jet; that is, the jet core velocity is decreasing with downstream distance such that the jet front has a lower velocity than the orifice exit flow.

The results obtained for liquid-segment method are discussed in this section. The jet instability problem simulated in the laboratory frame is now transferred to a new coordinate system accelerating consistent with liquid acceleration at the orifice exit obtained in the previous section (400,000 m/s^2). A small section of the jet, e.g., 1 mm with a 200-micron radius surrounded by air at 30 atm is considered. The liquid is initially quiescent

while the gas blows over the liquid from right to left. The gas initial velocity is consistent with the maximum velocity of the jet in the laboratory frame when its penetration length is about 1mm. The boundary conditions were described in the previous section. The initial velocity profile consists of a small thickness boundary layer for the liquid varying between zero to 80 m/s along 100-micron orifice radius combined with a large thickness boundary layer for the gas varying between 80 to 100 m/s along 300 μm in radial direction. The velocity profile of both phases along the radial direction has been shown in Figure 7 at different instants of time. The velocity of liquid and gas increases with time consistent with the constant acceleration of the frame of reference. The oscillations appear at the velocity profile at a later time is due to the surface instability and formation of liquid protrusions. As Figure 8 (upper) depicts, initial disturbances with 100 μm wavelength have been applied on the liquid/gas interface in observation of the effects of instabilities due to nozzle cavitation during injection.

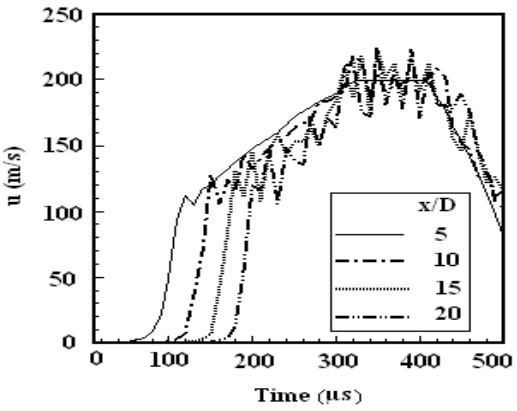

Figure 5. Jet centerline axial-velocity vs. time at different positions downstream of the orifice exit.

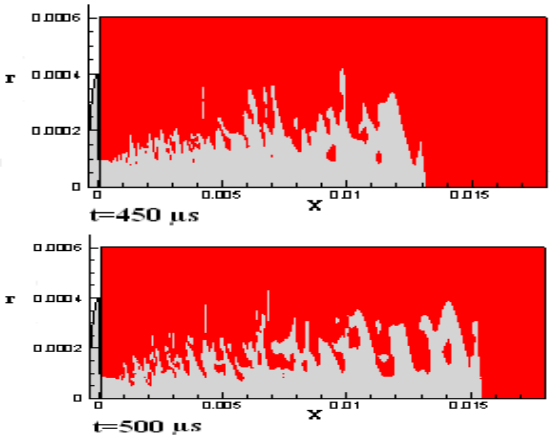

Figure 6. Simulated jet development during shut-down at two instants of time: 450 μs (up) and 500 μs (down).

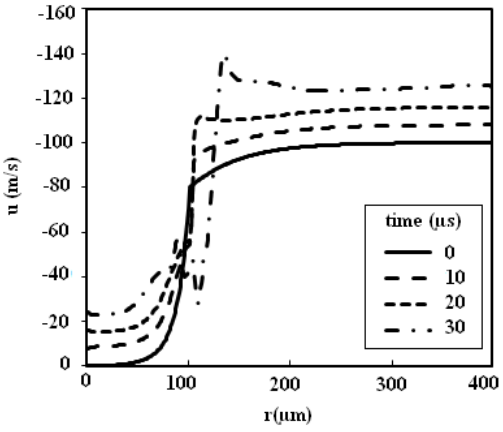

Figure 6. Liquid/gas velocity profile vs. radial direction for liquid-segment at different instants of time.

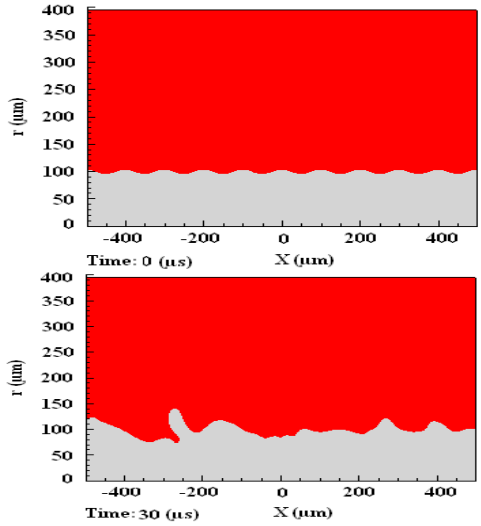

Figure 7. Initial disturbance (top), surface protrusions at t= 30 μs (bottom), Re=16,000, We=23,000.

Figure 8 illustrates the development of the unstable wavelengths at the liquid surface at two instants of time. The primary KH waves with wavelengths of 100-200 μm travel to upstream relative to the liquid (left) while their amplitude increases and long ligaments (fingers) are drawn out of liquid. These ligaments turn and roll-up in the flow direction (right to left). At the same time, they turn into a very thin film with a blob of liquid at the end. This phenomenon has been reported for droplets accelerated by a constant force in a quiescent environment for large accelerations [6]. In addition to the acceleration of the frame of reference, these ligaments are exposed to very high local accelerations normal to their interface that make them a good prey for small-scale RT instabilities (10-50 μm); these secondary instabilities appear at the edge of the ligaments formed by the primary

instabilities at the interface. Figure 10 illustrates the instabilities due to an acceleration which is two times those of Figure 9 at 40 and 50 μs after the start of injection while other parameters, i.e., Re and We numbers, remain constant. Increasing the acceleration of the frame of reference leads to the formation of longer and thinner ligaments with smaller RT wavelengths on their crests at comparable instants of time. It is instructive to investigate the effects of surface tension on jet instability. According to the viscous potential flow dispersion relation from Funada *et al.* [15] at sub-millimeter, super-micron wavelength range of interest, unlike gravity viscosity and surface tension are very important. Surface tension has stabilizing effects for smaller wavelengths; thus, at higher We numbers we expect smaller wavelengths**.** A comparison between Figure 10 and 11 depicts that at a comparable instant of time, i.e., 40 μs after the start of injection smaller waves and thinner ligaments appear at the liquid/gas interface for higher We number at constant acceleration and Re number.

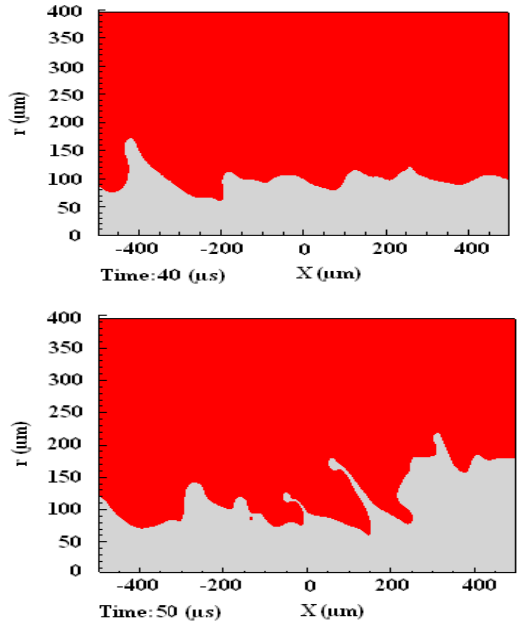

Figure 8. Instabilities at the gas/liquid interface for liquid-segment model at two instants of time t=40 μs (up), t=50 μs (down), Re=16,000, We=23,000, a= 400,000 m/s^2.

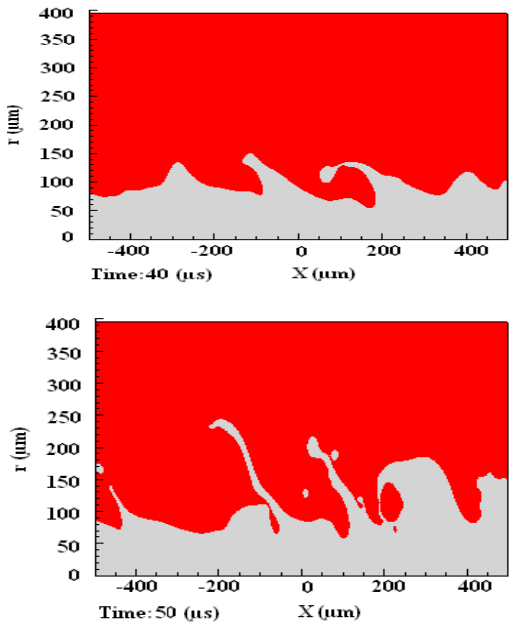

Figure 9. Instabilities at the gas/liquid interface for liquid-segment model at two instants of time t=40 μs (up), t=50 μs (down), Re=16,000, We=23,000, a=800,000 m/s^2.

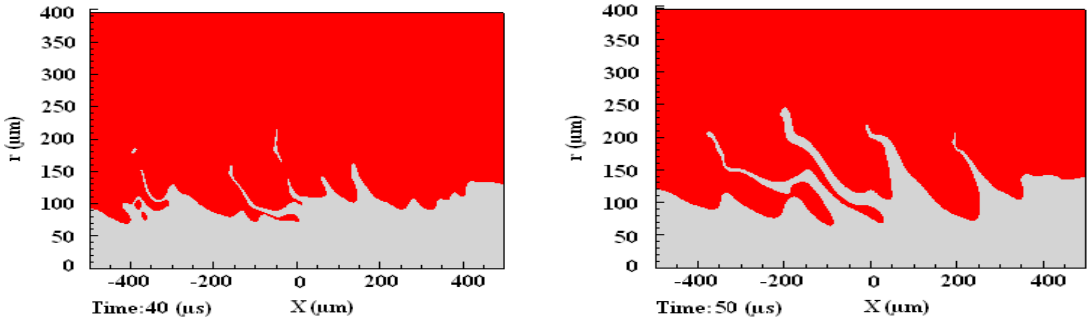

Figure 10. Instabilities at the gas/liquid interface for liquid-segment model at two instants of time t=40 μs (left), t=50 μs (right), Re=16,000, We=230,000, a= 800,000 m/s^2.

Different ligaments at the interface have been considered and their lengths, thicknesses, and the RT wavelengths have been measured and gathered in Table 2. On the other hand, the RT wavelengths have been compared with linear instability theories used in the literature [5,7]. Based on this theory, $\lambda_{RT} = 2\pi\sqrt{\frac{3\sigma}{\rho_l a}}$ where λ_{RT} is the RT instability wavelength and a, σ, and ρ_l are the local acceleration, surface tension coefficient, and

gas density, respectively. The measured results show a good agreement with predicted RT wavelengths. The discrepancies likely stem from the fact that the classical formulation neglects the effects of viscosity and nonlinearity of the problem.

Summary and Conclusions

The behavior of the liquid jet injected into air at 30 atm has been simulated during start-up and shut-down. Use has been made of an unsteady multidimensional code with a finite-volume solver of the Navier-Stokes equations for liquid streams and adjacent gas, a boundary-fitted-gridding scheme, and a level-set method for gas/liquid interface tracking. The simulation of the full jet depicts that, for lower Reynolds numbers, the starting liquid jet forms a cap which grows in volume as it moves downstream and decelerates along the gas chamber. However, for higher Reynolds numbers the mushroom-shaped cap disappears after a few microseconds after the start of injection and KH and RT inabilities develop on the liquid/gas interface. To tackle the resolution problem and capture the shortest unstable surface wavelengths, a new model has been developed to examine stream-wise segments of the jet during start-up and shut-down. The frame of reference has been transferred from the laboratory frame to an accelerating frame fixed to the liquid. This transformation generates a new term as a generalized body force analogous to gravity in equations of motion. The simulations show that the primary KH waves, in the order of 100-200 μm, travel to the upstream relative to the liquid mass while their amplitude increases and long ligaments are drawn out of the liquid. For higher We numbers, smaller waves and thinner ligaments appear at the liquid/gas interface with constant acceleration. These ligaments turn into a very thin film with a blob of liquid at the end. At high Re and We numbers small-scale wavelengths and protrusions become even smaller due to exposure to high accelerations normal to their interface. This leads to small-scale RT waves at the edge of the ligaments. The normal acceleration on the fingers is of the order of 10^6 m/s^2. A comparison between the computed RT wavelengths with classical linear instability theory probably shows a reasonable agreement. However, the measured wavelengths are higher compared to the theory due to the fact that the damping effects of viscosity on the smallest wavelengths have not been considered in the theory.

Table 2. RT wavelengths compared with theory.

T(μs)	L (μm)	Thickness (μm)	Avg. velocity (m/s)	a_{normal} (m/s^2)	RT wavelengths observed from computations (μm)	Predicted (μm) $\lambda_{RT}=2\pi\sqrt{\frac{3\sigma}{a\rho_l}}$
17	136.3	7.6-57.6	-64.3	2.35e6	53.1	37.91
18	100	5.6-18.9	-68.0	2.04e6	33.4 and 38.9	40.75
19	117.1	3-18.6	-71.6	4.07e6	35.7	28.85

Acknowledgements

The authors gratefully acknowledge support from The U.S. Army Research Office through Grant No. W911NF-09-1-0208 with Dr. Ralph A. Anthenien Jr. as the Program Manager of Propulsion and Energetiscs.

References

[1] Herrmann, M., *Journal of Computational Physics* 227: 2674-2706 (2008).
[2] Goroshovski, M., Herrmann, M., *Annual Review of Fluid Mechanics* 40: 343-366 (2008).
[3] Linne, J. M., Paciaroni, M. Hall, T., and Parker, T., *Experiments in Fluids* 40: 836–846 (2006).
[4] Sazhin, S. S., Turner, M. R., Healey, J. J., and Martynov, S. B., *ILASS, European Conference on Liquid Atomization and Spray Systems*, Estoril, Portugal, September 2011.
[5] Joseph, D. D., Belanger, J., Beavers, G. S., *International Journal of Multiphase Flow* 25:1263-1303 (1999).
[6] Han, J., Tryggvason, G., *Physics of Fluids* 11(12): 3650-3667 (1999).
[7] Varga, C. M., Lasheras, J. C., and Hopfinger, E. J., *Journal of Fluid Mechanics* 497:405-434 (2003).
[8] Jarrahbashi, D., Sirignano, W. A., and Dabiri, S., *ILASS Meeting*, Ventura, CA, May 2011.
[9] Hayase, T., Humphrey, J. A. C., and Greif, R., *Journal of Computational Physics* 98, 1:108-118 (1992).
[10] Patankar, S. V., *Numerical Heat Transfer and Fluid Flow*, Hemisphere, Washington, DC, 1980.
[11] Sussman, M., Fatemi, P., Smereka, E. P, and Osher, S., *Computers and Fluids* 27:663-680 (1998).
[12] Osher, S., Fedkiw R. P., *Journal of Computational Physics* 169: 436-502 (2001)
[13] Dabiri, S., Sirignano, W. A., and Joseph, D. D., *Journal of Fluid Mechanics* 605: 1-18 (2008).
[14] Abani, N., Ghandhi, J. B., and Reitz, R. D., *Conference on Thermo- and Fluid Dynamic Processes in Diesel Engines* (2008).
[15] Funada, T., Joseph D. D., *Journal of Fluid Mechanics*, 445: 263-283. (2001).